Modern control strategies of doubly-fed induction generator based wind turbine system

Zhou, Dao; Song, Yipeng; Blaabjerg, Frede

Published in:
Chinese Journal of Electrical Engineering

DOI (link to publication from Publisher):
10.23919/CJEE.2016.7933112

Publication date:
2016

Document Version
Publisher's PDF, also known as Version of record

Modern Control Strategies of Doubly-Fed Induction Generator Based Wind Turbine System

Dao Zhou, Yipeng Song, and Frede Blaabjerg[*]

(Aalborg University, Aalborg, 9220, Denmark)

Abstract: A doubly-fed induction generator(DFIG) based configuration is still preferred by wind turbine manufacturers due to the cost-effective power converter and independent control of the active power and reactive power. To cope with stricter grid codes(e.g. reactive power compensation, low voltage ride-through operation, as well as steady and safe operation during long-term distorted grid), control strategies are continuously evolving. This paper starts with a control strategy using the combined reactive power compensation from both the back-to-back power converters for their optimized lifetime distribution under normal grid conditions. Afterwards, an advanced demagnetizing control is proposed to keep the minimum thermal stress of the rotor-side converter in the case of the short-term grid fault. A modularized control strategy of the DFIG system under unbalanced and distorted grid voltage is discussed, with the control targets of the smooth active and reactive power or the balanced and sinusoidal current of the rotor-side converter and the grid-side converter. Finally, a bandwidth based repetitive controller is evaluated to improve the DFIG system's robustness against grid frequency deviation.

Keywords: Doubly-fed induction generator, reactive power, low voltage ride-through, unbalanced and distorted grid.

1 Introduction

A recent study by the Danish Energy Agency indicates that onshore wind power is the cheapest form of new electricity generation in Denmark[1]. Meanwhile, due to noise emission, footprint limitation and requirement for more wind energy, interest in offshore wind turbines has been increasing, where lifespan is expected to be 20~25 years[2]. As one of the most vulnerable components of the wind turbine system, much effort has been devoted to the reliable behavior of the power electronic converter because of the increased cost and time for offshore maintenance[3]. Furthermore, it is generally accepted that the thermal profile of the power semiconductor is an important indicator of the lifespan and has an influence on the reliability metrics[4-5].

A doubly-fed induction generator(DFIG) structure is still the most used concept by wind turbine manufacturers due to the cost-effective power converter and the independent control of the active power and reactive power[6-8]. However, stricter grid codes on the low voltage ride-through (LVRT) prevent widespread use of this concept as the direct connection between the stator and power grid, causing high rotor voltage which may result in the overvoltage and overcurrent of the rotor-side converter in back-to-back power converters. At the same time, emerging grid codes require wind farms to withstand a small 2% steady-state voltage unbalance and higher transient unbalance without tripping[9].

To cope with the modern grid codes, this paper introduces a series of control strategies in cases of normal grid condition, short-term grid fault and long-term distorted grid. In section 2, a control strategy of the combined reactive power compensation from back-to-back power converters is described seen from their optimized lifetime distribution under normal grid condition. In the case of short-term grid fault, hardware and software solutions of the DFIG system are addressed, and an advanced demagnetizing control is proposed to minimize thermal stress of the rotor-side converter. The control strategy under long-term unbalanced and harmonic grid is investigated to improve the DFIG system performance such as balanced and sinusoidal current or smooth output active power and reactive power. A bandwidth based repetitive controller is proposed to improve the robustness of the control strategy against the grid frequency deviation by using the bandwidth parameter compared to the conventional repetitive controller. Finally, some concluding remarks are drawn in Section 6.

2 Reactive power control in normal grid condition

As wind turbines are usually located in remote areas, the voltage amplitude at the end of the transmission line may not be steady and robust enough. More countries have recently issued new regulations with respect to wind power management[10-11]. For instance, German grid code specify the relationship between active power production and reactive power injection as shown in Fig.1[11]. Even though the power grid operates normally (i.e. without voltage dip or harmonic distortion), if the active power is generated higher than 0.2pu, up to 0.4pu over-excited and 0.3pu under-excited reactive power is required and preferred.

* Corresponding Author, E-mail: fbl@et.aau.dk.

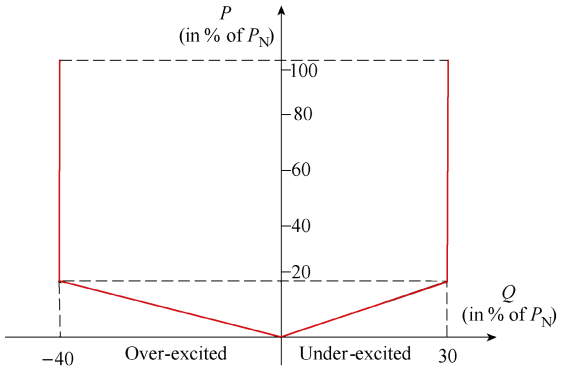

Fig.1 Reactive power support stated in the German grid code

The configuration of the DFIG system is shown in Fig.2, in which power converters are termed the grid-side converter (GSC) and the rotor-side converter (RSC) due to their positions. Apart from the advantage of being a cost effective and efficient power electronic converter, the reactive power has two injection routes fed back to the power grid. The stator of the DFIG stator Q_s and the GSC Q_g are different solutions, and can be independently controlled by the RSC and the GSC.

Since the rotor voltage referred to the stator side is almost the product of the stator voltage and DFIG's slip value, taking the winding ratio of the stator and rotor into account, the rated rotor voltage can still be estimated to be much lower than the stator voltage due to the low value of the rated generator slip. Assuming the same winding ratio of the primary, secondary and tertiary side in the grid-connected transformer, the RSC output voltage is much lower than the interfacing voltage of the GSC. The same active power through the back-to-back power converter leads to a de-rated design in order to maintain similar current stress of each power module at the rated power.

In the case of the stator voltage orientation under the dq-reference frame, the DFIG stator-side voltage vector can be estimated, and the current vector can be calculated during the fixed active power generation and the reactive power injection. If all quantities are transferred to the rotor side, the DFIG rotor-side current vector and voltage vector can be expressed by the stator-side current and voltage.

$$\begin{aligned}\boldsymbol{i}_r &= i_{rd} + \mathrm{j}i_{rq} \\ &= -k_{sr}\frac{X_s}{X_m}i_{sd} + \mathrm{j}k_{sr}\,\mathrm{sign}(s)\left(-\frac{u_{sd}}{X_m} - \frac{X_s}{X_m}i_{sq}\right)\end{aligned} \tag{1}$$

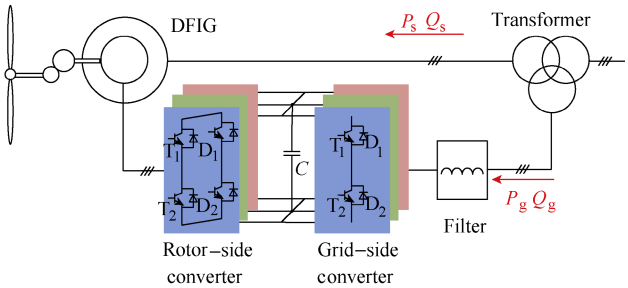

Fig.2 Control possibility of reactive power in DFIG system

$$\begin{aligned}\boldsymbol{u}_r &= u_{rd} + \mathrm{j}u_{rq} \\ &= \frac{s}{k_{sr}}\left(\frac{X_r}{X_m}u_{sd} + \frac{\sigma X_r X_s}{X_m}i_{sq}\right) - \mathrm{j}\frac{\mathrm{sign}(s)}{k_{sr}}\left(s\frac{\sigma X_r X_s}{X_m}i_{sd}\right)\end{aligned} \tag{2}$$

where X_s, X_m and X_r denote the stator reactance, the magnetizing reactance, and the rotor reactance respectively; σ denotes the leakage coefficient, defined as $(X_sX_r-X_m^2)/X_sX_r$; s denotes the slip value of the induction generator; k_{sr} denotes the winding ratio between the DFIG stator-side and the rotor-side, and subscripts dq denote the variable in d-axis and q-axis. Due to the positive sequence of rotor variables during the sub-synchronous mode, but negative sequence during the super-synchronous mode, the function sign(s) is introduced, meaning if the slip value is positive, its value becomes 1. Alternatively, if the slip value is negative, its value becomes −1.

Similarly, if a single inductor is used as the filter, the converter output current $\boldsymbol{i}_c$ and voltage $\boldsymbol{u}_c$ can be expressed by the grid current $\boldsymbol{i}_g$ and voltage $\boldsymbol{u}_g$.

$$\boldsymbol{i}_c = i_{cd} + \mathrm{j}i_{cq} = i_{gd} + \mathrm{j}i_{gq} \tag{3}$$

$$\boldsymbol{u}_c = u_{cd} + \mathrm{j}u_{cq} = (u_{gd} - X_g i_{gq}) - \mathrm{j}X_g i_{gd} \tag{4}$$

where X_g denotes the filter reactance.

In the case of the voltage orientation, the reactive power injection affects the current value in q-axis regardless of the DFIG stator-side or the GSC converter current. According to (1)~(4), it can be seen that the injection of the reactive power not only changes the current amplitude of the converter, but also modifies the converter output voltage.

With the parameters of a 2MW DFIG system listed in Table 1, 1kA/1.7kV power module is used and the DC-link voltage is kept at 1050V, and the reactive power effect to the back-to-back power converters is shown in Fig.3. Three different wind

Table 1 Parameters for 2MW DFIG

DFIG	
Parameters	Values
Rated power P_s/kW	−2000
Rated stator frequency f_1/Hz	50
Rated slip value s	−0.2
Stator peak phase voltage u_{sd}/V	563
Stator reactance X_s/Ω	0.93
Magnetizing reactance X_m/Ω	0.91
Rotor reactance X_r/Ω	1.00
Turns ratio k_{sr}	0.369
Power converter	
Rated power/kW	400
DC-link voltage U_{dc}/V	1050
Switching frequency f_s/kHz	2
Power modules used in GSC	1 kA/1.7kV, single
Power modules used in RSC	1 kA/1.7 kV, two in parallel
Grid filter	
Grid peak phase voltage u_{gd}/V	563
Filter reactance X_g/Ω	0.16

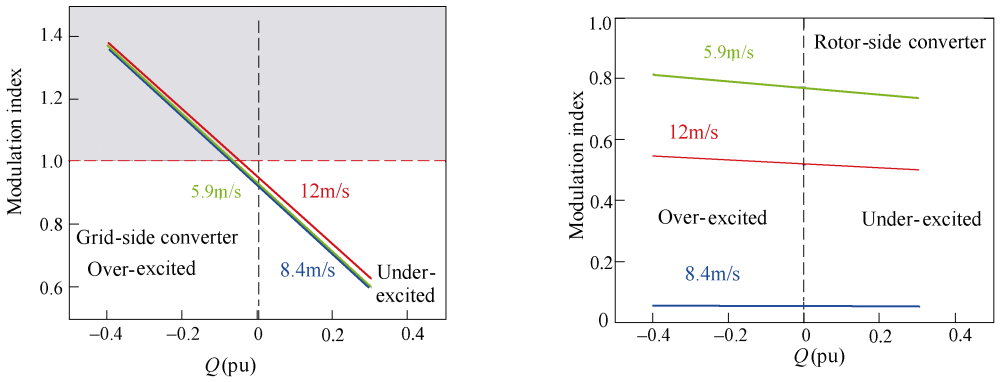

(a) Modulation index

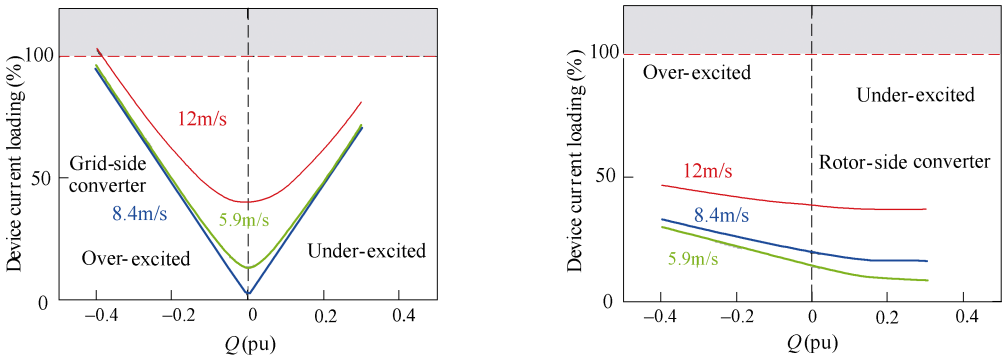

(b) Current loading of the device

Fig.3 Effects of the reactive power injection to back-to-back power converters of a 2MW DFIG system

speeds present the super-synchronous, the synchronous and the sub-synchronous operation of the DFIG. It is noted that the modulation index and device current loading change significantly if the reactive power is compensated from the GSC, while the modulation index and device current loading is kept almost the same in the case that the varying degrees of reactive power are controlled by the RSC.

Based on the converter current and voltage, together with the phase angle between them, the loss dissipation of each power semiconductor can be calculated. According to the thermal model of the power semiconductor, the thermal profile can be mapped in terms of various wind speeds. On the basis of the released lifetime model from power semiconductor manufacturers, which tests and identifies how many power cycles the power semiconductor can withstand at different levels of thermal stress, the annual consumed lifetime can be estimated on the basis of annual wind profile.

Due to the lower operation frequency of the RSC compared to the GSC, its lifetime is much shorter because of the higher thermal stress[12]. As the over-excited reactive power exacerbates current and voltage stress of the RSC, the injection of the over-excited reactive power becomes critical from the system lifetime point of view. A combined reactive power injection from both the GSC and the RSC can be proposed in order to balance the lifetime between the back-to-back power converters, thereby enhancing the reliability of the DFIG system.

Considering the different wind classes[13], the lifetime of the RSC and the GSC can be compared at different compensation strategies as shown in Fig.4. It is proven that the total consumed lifetime remains almost constant in a log-scale at different compensation schemes from the RSC point of view, while the total consumed lifetime varies significantly for the GSC. Moreover, it can be seen that the most balanced lifetime between the RSC and the GSC appears to be in the case that 0.1pu over-excited reactive power is supported by the RSC, and 0.3pu is provided by the GSC. For instance, the total consumed lifetime of the RSC can be optimized from 3.59E-2 to 2.50E-2 in Class I wind profile, which implies 1.5 times enhanced lifespan.

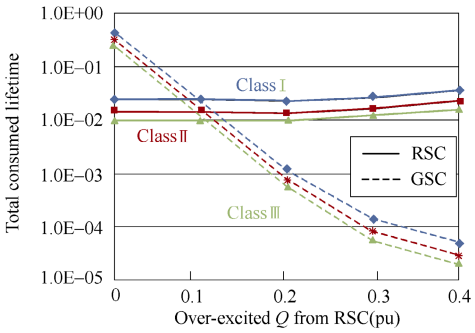

Fig.4 Total consumed lifetime among the different reactive power compensation strategies, in which the various wind classes are taken into account

Note: The solid line indicates the diode of the rotor-side converter, and the dot line indicates the IGBT of the grid-side converter; Color blue, red and green indicate the wind Class I, Class II and Class III, respectively

3 Ride-through control during short-term fault

With increasing penetration, wind turbines are no longer allowed to disconnect from the power grid as that may easily create instability in the power system. Modern grid codes require that the DFIGs not only remain linked to the grid, but also inject the reactive current to support its recovery. For instance, the specification of German grid code is shown in Fig.5.

As the stator of the DFIG is directly connected to the grid, the sudden change of the grid voltage may induce the natural stator flux (balanced fault) and even negative stator flux (unbalanced fault). Viewed from the stator reference frame, the vector of a natural stator flux stands still, while the vector of the negative stator flux rotates at the twice speed of the grid angular frequency. As a consequence, both rotate at a much higher frequency than the positive stator flux of the slip angular frequency at the rotor reference frame, which implies that the occurrence of the natural and negative stator flux leads to significant increase of the rotor voltage. The sufficiently high rotor voltage may saturate the RSC, causing its over-voltage and even over-current.

In order to support the DFIG to successfully ride through the grid fault, both hardware solutions and software solutions can be used. As shown in Fig.6, in the case of the grid fault, a crowbar is activated and short-circuits the rotor winding through resistors, thereby limiting the rotor voltage and providing an additional path of rotor current. Meanwhile, the rotor current continues flowing into the converter DC-link through the freewheeling diode of the RSC. A dc-chopper is equipped to take care of the remaining wind power and prevent the fast increase of the DC-voltage. However, in addition to the cost impact of the hardware, the DFIG behaves as a squirrel-cage induction motor during the activation period of the crowbar and absorbs the reactive power from the power grid, contradictory to grid code requirements.

Advanced control strategies are an important and cost-effective solution for the DFIG ride-through operation. One popular approach is to use demagnetizing current control as shown in Fig.7, which switches the

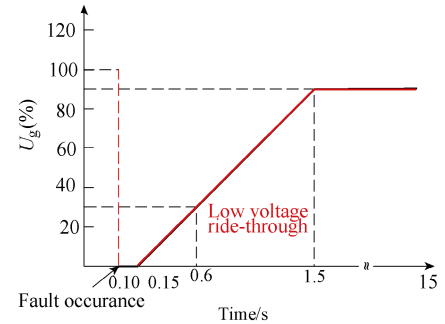

(a) Low voltage ride-through

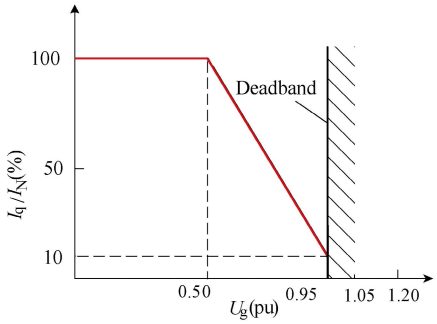

(b) Reactive current injection

Fig.5 Wind turbine requirements under grid disturbance

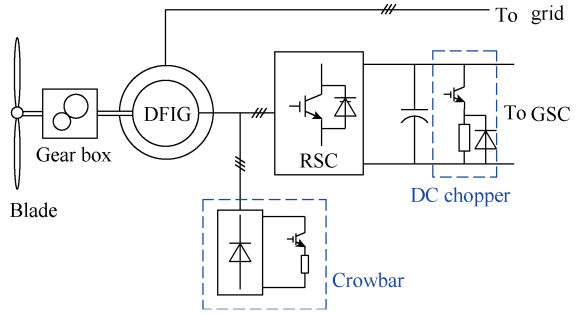

Fig.6 Auxiliary hardware of DFIG during the grid fault ride-through

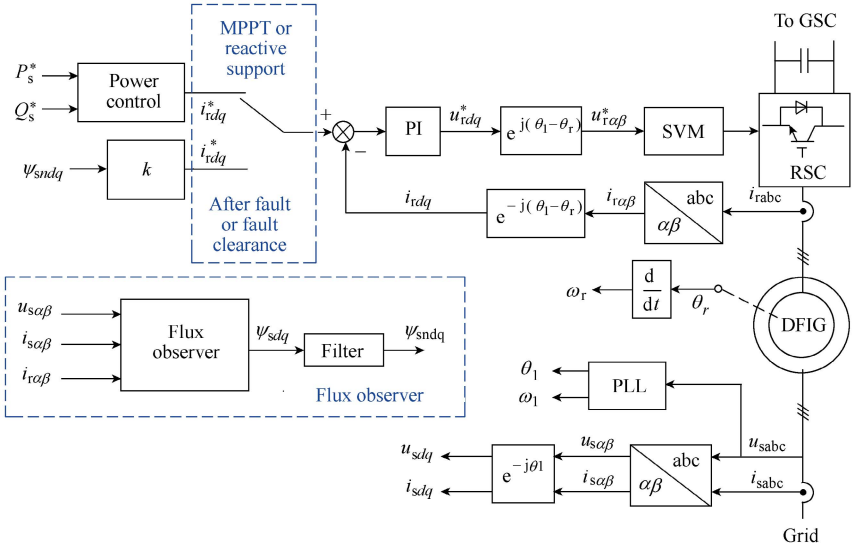

Fig.7 Demagnetizing control strategies during the grid fault ride-through

control target from the active power and the reactive power to the natural component of the stator flux. Compared to the vector control, a flux observer and a notch-filter are employed to extract the natural component of the stator flux. By using the demagnetizing current control, the decaying of the natural stator flux can be accelerated, and the induced rotor voltage can be reduced[15-16].

According to the capacity of the RSC, the demagnetizing coefficient can maximally be designed in order to minimize decay of the natural stator flux[15]. However, viewed from the thermal stress of the power semiconductor, the optimum situation is to keep the rotor current low enough. Considering the grid code at the instant and amount of reactive current injection, the demagnetizing coefficient can be designed in order to equalize the rotor current between the instant of the grid fault and the instant of the reactive current injection[16].

In order to prevent the power module from a too high DC-link voltage, a DC-brake is used in the simulation, whose threshold values for turn-on and turn-off the switch are set at 1300V and 1100V by using a hysteresis control. Assuming that a 0.7 balanced grid voltage dip occurs at the instant of 0.5s, a comparison between the traditional vector control and optimized demagnetizing current control are shown in Fig.8, in which the DFIG operates with rotor speed at 1800r/min.

For the traditional vector control in Fig.8(a), once the grid fault is detected, both the active current and reactive current are set to zero. However, due to the existence of the natural flux, the rotor current (i_{rd} and i_{rq}) cannot track the reference of the rotor current (i_{rd}^* and i_{rq}^*), and the enable time of the dc chopper lasts almost 90ms. Moreover, in accordance with the grid codes, a 1.0pu reactive current is injected at the instant of 0.65s, and the maximum junction temperature of the diode appears during the period without the reactive current injection, which reaches almost 93.0℃.

As shown in Fig.8(b), when the grid fault occurs, a demagnetizing current is selected. During the fault period, the rotor current is kept closely within the desired value, and the enable time of the dc chopper is reduced to 35ms. Compared with the period of demagnetizing control and reactive current injection, it is noted that the diode is almost equally stressed and its maximum junction temperature is reduced to 90.0℃. Furthermore, the damping of the stator flux ψ_s is much faster than the traditional vector control. Above all, it is noted that a proper design of the demagnetizing coefficient is able to achieve a minimal thermal stress during the period of the grid fault.

4 Control strategy under long-term unbalanced and harmonic grid

As an increasing amount of unbalanced/non-linear loads and power generation units are connected to the grid network, a long-term three phase unbalanced voltage with harmonic distortion may consequentially be produced. The overall performance of the DFIG system can deteriorate, i.e., including the unbalanced and distorted stator current, the pulsated active,

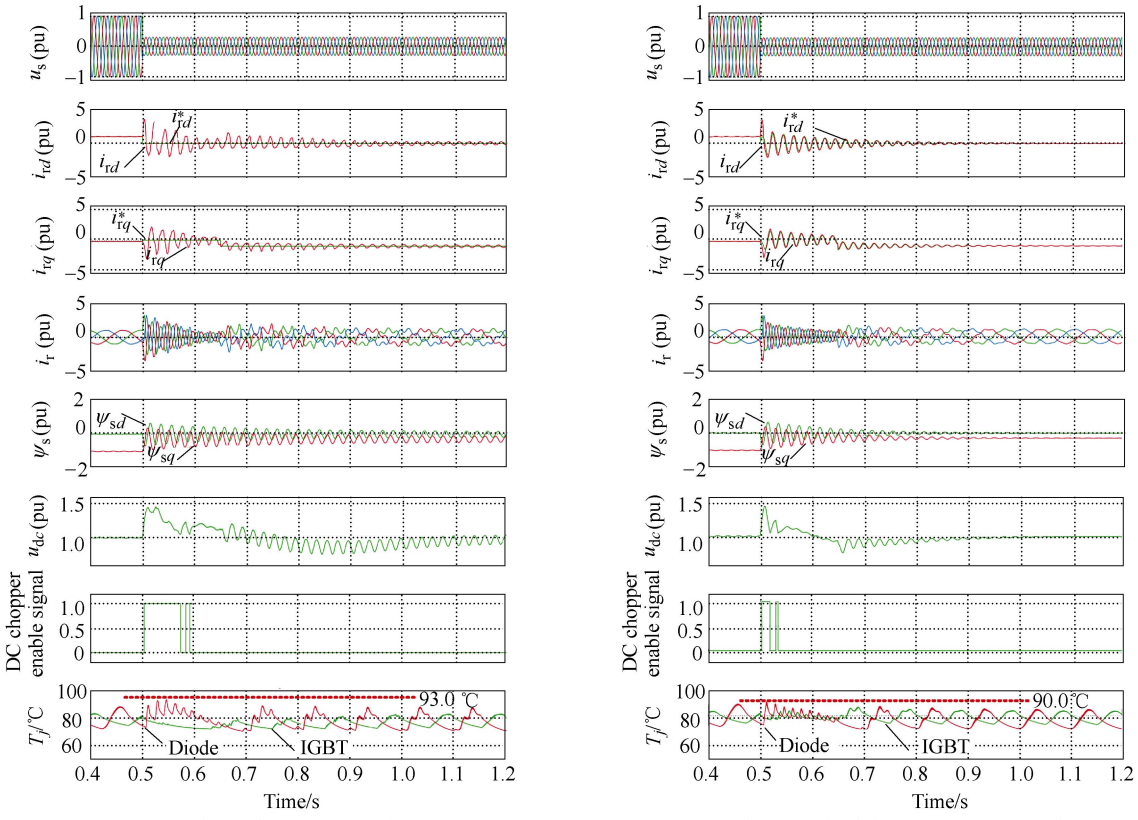

(a) Traditional vector control (b) Optimized demagnetizing control

Fig.8 Simulated results in the case of the DFIG at 1800r/min to ride through 0.7 dip balanced grid fault with various control schemes

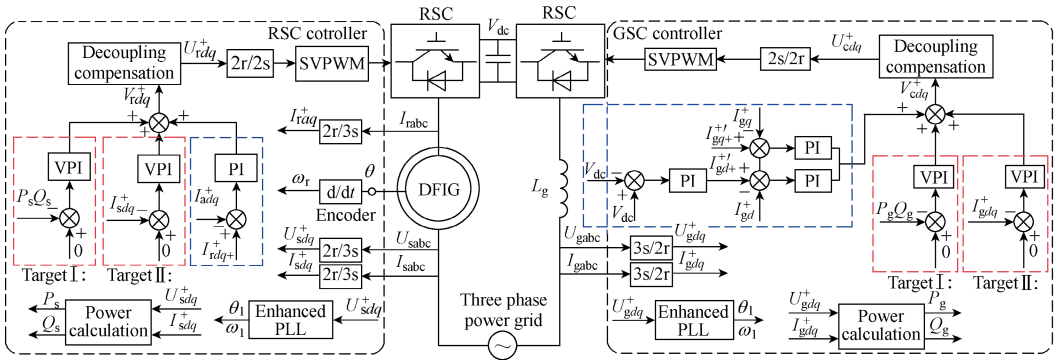

Fig.9 Block diagram of the proposed modularized control strategy of DFIG system

reactive power and electromagnetic torque. Thus, for the purpose of improving DFIG behavior under long-term unbalanced and harmonic grid, an effective control strategy needs to be implemented.

During normal operation, the DC link voltage V_{dc} is able to maintain stability, thus allowing the RSC and GSC of the DFIG to operate independently as two separate modules without any communication. This modularized control strategy and its block diagram of the DFIG are shown in Fig.9. From the perspective of delivering wind energy with acceptable quality, the two control targets for the DFIG system can be defined as,

1) Target I: No pulsation of active and reactive power delivered to the power grid.

2) Target II: No negative and harmonic components of current injected into the power grid.

With respect to the control strategy of the RSC, the phase angle of the grid voltage θ_1 can be obtained by the enhanced phase locked loop (PLL) module[18-25] based on the resonant regulator tuned at 100Hz and 300 Hz, while the rotor position θ_r can be obtained from the encoder. Afterwards, the DFIG stator active and reactive power P_s and Q_s can be calculated based on the stator voltage U^+_{sdq} and stator current I^+_{sdq}.

The closed-loop control of the rotor current I^+_{rdq} can be realized based on a conventional PI regulator with the aim of the DFIG average power. In the case where alternative control targets are chosen, (i.e., smooth active and reactive power output or balanced and sinusoidal stator current), the closed-loop control with the vector proportional integral (VPI) controller tuned at 100Hz and 300Hz is employed to directly regulate the negative and harmonic components of the stator current, or the 100Hz and 300Hz pulsation of stator output active and reactive power.

With respect to the control strategy of the GSC, the active and reactive power of the GSC P_g and Q_g can be calculated according to the sampled grid voltage U^+_{gdq} and current I^+_{gdq}. Since the major function of GSC is to provide a stable DC-link voltage V_{dc}, the closed-loop control of DC-link voltage is implemented based on a PI regulator, and its output is considered as the d-axis current reference I^{+*}_{gd+}. Together with the q-axis current reference I^{+*}_{gq+} (normally set 0 for unity power factor operation), both of them are used as the input of current PI controller to regulate the positive component of the grid current.

Similar to the RSC control, considering the alternative control targets (i.e., the smooth GSC active and reactive power or the balanced and sinusoidal GSC current), the closed-loop control with the VPI regulator tuned at 100Hz and 300Hz is adopted to directly regulate the GSC current negative and harmonic components, or the 100Hz and 300Hz pulsations of the GSC active and reactive power.

A laboratory prototype of the down-scale 1kW DFIG system was set up and shown in Fig.10. The DFIG is driven by a 1.5kW squirrel cage induction machine as the wind turbine, which is driven by a general converter. The ac source Chroma 61704 is employed to emulate the unbalanced and distorted power grid. During the experiment, the negative, 5th and 7th order harmonic components of the grid voltage are set at 2.90%, 2.36% and 1.17% respectively. The parameters of the DFIG system are listed in Table 2.

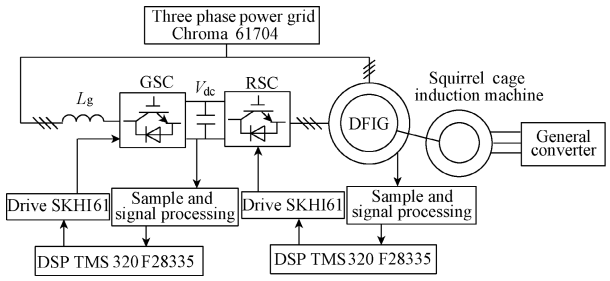

Fig.10 Laboratory prototype of 1kW down-scale DFIG system

Table 2 Parameters of experimental DFIG system

DFIG	
Rated power P_s/kW	−1
Rated stator frequency f_1 /Hz	50
Grid RMS line voltage u_{sd} /V	110
Stator resistance R_s/Ω	1.01
Rotor resistance R_r/Ω	0.88
DFIG mutual inductance L_m/mH	90.1
DFIG stator leakage inductance $L_{\sigma s}$/mH	3.0
DFIG rotor leakage inductance $L_{\sigma r}$/mH	3.0
Turns ratio k_{sr}	0.33
Pole pairs of DFIG n_p	3
Power converter	
DC-link voltage V_{dc} /V	200
Switching frequency f_s/kHz	5
Grid filter	
GSC line inductance L_g/mH	4
GSC line resistance R_g/Ω	0.02

Regarding the control of the DFIG RSC, the rotor speed is initially set to 800r/min (the synchronous speed is 1000r/min), and the DC-link voltage is provided by the GSC at 200V. The control strategies for both the RSC and GSC are implemented using two separate DSP TMS320F28335 and a SEMIKRON SKHI61 for the driver for the IGBT. The sampling frequency is 10 kHz, while the switching frequency is 5 kHz.

Fig.11 shows the experimental results of the DFIG system under unbalanced and distorted grid voltage condition without the VPI regulator. It can be seen that significantly unbalanced and distorted current appears in both the GSC and the DFIG, and a 100Hz and 300Hz pulsation of the GSC and DFIG stator power can be observed. A detailed experiment result analysis can be summarized in Table III with the description of unbalanced and harmonic components.

Fig.12 shows experimental results of the DFIG system under unbalanced and distorted grid voltage condition with Fig.12(a) control target I and Fig.12(b) control target II. As seen from Fig.12(a), when the control target I is implemented, both the GSC power and the DFIG stator power become much smoother. As summarized in Table III, in order to eliminate the 100 Hz GSC power and DFIG stator power pulsation, both the GSC current and DFIG stator current contain a non-negligible amount of the 3rd harmonic component.

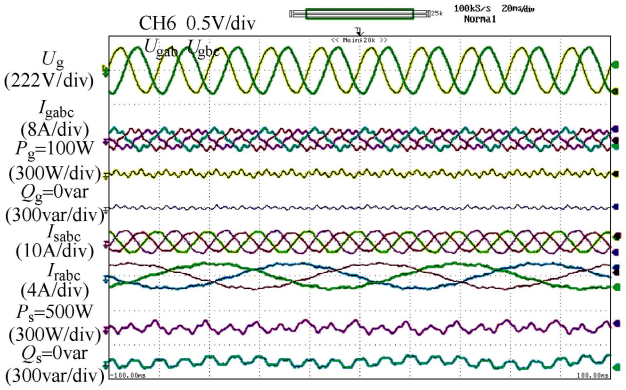

Fig.11 Experimental results of DFIG system performance under unbalanced and distorted grid voltage condition when VPI regulator is disabled

Similarly, for the purpose of 300Hz power pulsation removal, the GSC current and DFIG stator current contain the severe 5th and 7th harmonic components.

Fig.12(b) presents experimental results of DFIG system under the unbalanced and distorted grid voltage condition with the control target II, i.e., the balanced and sinusoidal GSC current and DFIG stator current can be achieved. Both the GSC current and DFIG stator current are significantly improved with negligible harmonic distortion and minimal unbalance, which contributes to the safe and reliable operation of the power grid. As well, the pulsation of the GSC power and DFIG stator output power can be higher than that of the control target I.

It can be observed from Table 3 that, compared to the control without the VPI regulator, the unbalanced and distorted current, as well as power pulsation can be significantly improved whatever control target is implemented. Moreover, the pulsation of the DFIG stator output active/reactive power and GSC active/ reactive power under the control target I is much lower than that of the control target II. However, the distorted DFIG stator current and GSC current, containing 3rd, 5th and 7th harmonic components, can be generated as a consequence. It should be noted that the negative component of DFIG stator current or GSC current can be suppressed considerably by using both control targets.

Based on the aforementioned experimental results, it can be found that when the DFIG system operates during the unbalanced and harmonic voltage, the advantages of the proposed control strategy compared with conventional coordinated control strategy can be concluded as,

1) In order to achieve the two alternative control targets, both the RSC and the GSC are able to operate independently without any communication, thus the control complexity of the DFIG system can be simplified.

2) The negative and harmonic components extraction of the grid voltage, stator current for the RSC or the grid current for the GSC can be avoided, and the complicated control reference calculation is also unnecessary. Therefore, the control complexity of the RSC and GSC can be reduced.

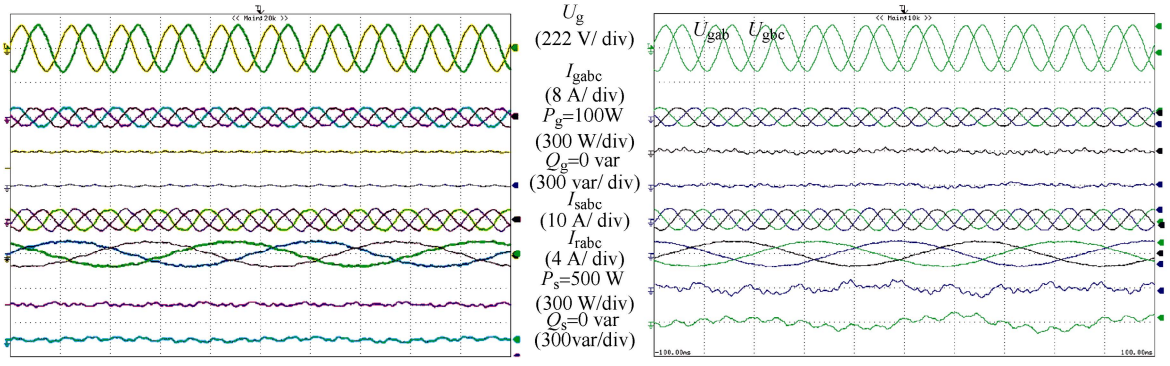

(a) Control target I

(b) Control target II

Fig.12 Experimental results of DFIG system under unbalanced and distorted grid voltage condition with control target I and control target II

Table 3 Analysis of experimental results

	Without VPI control	Control target I	Control target II
U_g negative	2.90%	2.90%	2.90%
U_g 250 Hz	2.36%	2.36%	2.36%
U_g 350 Hz	1.17%	1.17%	1.17%
I_g negative	13.82%	1.22%	1.62%
I_g 150 Hz	1.62%	4.70%	1.18%
I_g 250 Hz	14.49%	6.02%	2.31%
I_g 350 Hz	13.39%	2.88%	1.84%
P_g 100 Hz	±84 W	±10 W	±27 W
Q_g 100 Hz	±18 var	±9 var	±15 var
P_g 300 Hz	±36 W	±5 W	±30 W
Q_g 300 Hz	±30 var	±4 var	±24 var
I_s negative	17.42%	1.56%	1.69%
I_s 150 Hz	0.45%	5.41%	0.31%
I_s 250 Hz	4.37%	2.79%	1.85%
I_s 350 Hz	1.87%	2.01%	0.92%
P_s 100 Hz	±84 W	±18 W	±45 W
Q_s 100 Hz	±75 var	±25 var	±45 var
P_s 300 Hz	±36 W	±12 W	±30 W
Q_s 300 Hz	±24 var	±10 var	±21 var

3) By using the proposed control strategy, the control reference calculation for both the RSC and the GSC is no longer necessary. As DFIG system parameters are not involved in the control reference calculation, the possibility of DFIG system parameters deviation to affect the control accuracy can be eliminated.

5 Bandwidth based repetitive control in deviated grid frequency

Apart from the common low order 5th and 7th harmonic sequences, the power grid may also suffer from high order harmonic sequences such as 11th, 13th, 17th and 19th. In order to remove the harmonic components of the stator current under generalized harmonic voltage (including both low and high harmonic sequences), the repetitive control (RC) regulator can be adopted due to its advantage of controlling the multiple times of harmonic sequence at the same time. However, the conventional RC regulator is very sensitive to grid frequency deviation due to its small effective control bandwidth at the harmonic frequency. Thus, an improved RC regulator, i.e., the bandwidth based repetitive control (BRC) regulator with the introduction of the resonance bandwidth parameter, can be employed to enhance the RC regulator's robustness against the grid frequency deviation.

The conventional RC regulator in the discrete domain can be presented as

$$G_{\mathrm{rcz}}(z)=k_{\mathrm{rc}}\frac{Q(z)z^{-N}}{1-Q(z)z^{-N}} \tag{5}$$

$$Q(z)=(1-D)+Dz^{-1} \tag{6}$$

where, D is equal to the fractional part of $N_0/6$, and N_0 is the ratio of the sampling frequency to the grid fundamental frequency[17]. The delay N is set to the integral part of $N_0/6$. It has been proven in [17] that the block $Q(z)z^{-N}$ is capable of maintaining very good repetitive control performance when one-sixth of the ratio N_0 is non-integer.

With a certain mathematical deduction[18], the BRC regulator can be presented as

$$\begin{aligned}G_{\mathrm{brczPI}}(z)&=\frac{k_{\mathrm{rcb}}}{\dfrac{2}{T_0}\dfrac{1}{\dfrac{Q(z)z^{-N}}{1-Q(z)z^{-N}}}+\omega_{\mathrm{c}}}\\&=\frac{k_{\mathrm{rcb}}T_0Q(z)z^{-N}}{2\left(1-Q(z)z^{-N}\right)+\omega_{\mathrm{c}}T_0Q(z)z^{-N}}\end{aligned} \tag{7}$$

where, ω_{c} is the bandwidth in the proposed BRC regulator, T_0 is the period of fundamental control frequency, k_{brc} is the gain parameter of BRC regulator to adjust the magnitude response at the frequency of interest.

Fig.13 shows the bode diagram of conventional RC and proposed BRC regulators within the frequency from 298Hz to 302Hz, with grid frequency deviation of (50±0.2)Hz (i.e., (300±1.2)Hz). As shown in Fig.13, the conventional RC regulator and proposed BRC regulator with different bandwidth have different response when the grid frequency deviation happens.

For the conventional RC regulator (ω_{c}=0rad/s), the magnitude response drops from 40dB to 24dB, which may deteriorate the suppression capability of the stator current harmonic as a result of the higher steady-state control error. In the case of the proposed BRC regulator, its magnitude response drops from 40 dB to 29dB with bandwidth ω_{c}=2rad/s, and similarly from 40dB to 33dB with ω_{c}=5rad/s, from 40dB to 37 dB with ω_{c}=10rad/s. Therefore, it can be found that when the bandwidth ω_{c} is introduced to the conventional

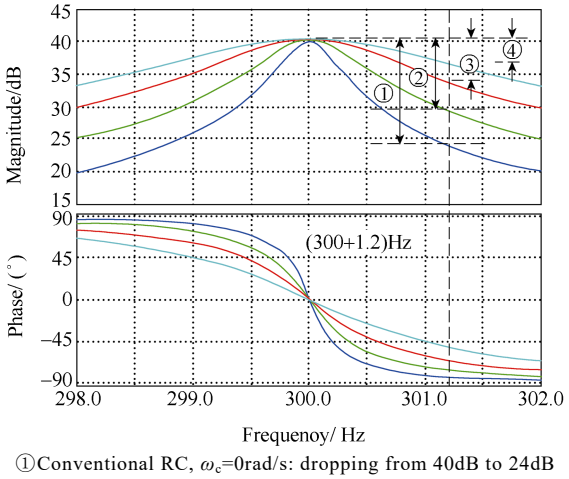

①Conventional RC, ω_{c}=0rad/s: dropping from 40dB to 24dB
②BRC regulator, ω_{c}=2 rad/s: dropping from 40dB to29dB
③BRC regulator, ω_{c}=5 rad/s: dropping from 40 dB to 33 dB
④BRC regulator, ω_{c}=10 rad/s: dropping from 40 dB to 37 dB

Fig.13 Bode diagram of conventional RC regulator $G_{\mathrm{rcz}}(z)$ and proposed BRC regulator $G_{\mathrm{brcPI}}(z)$. ($Q(z)$=2/3+1/3*z^{-1}, T_0=1/300 s and N=33; k_{brc}=250 when ω_c= 0 rad/s; k_{brc}=460 when ω_{c}=2 rad/s; k_{brc}=820 when ω_{c}=5 rad/s; k_{brc}=1300 when ω_{c}=10 rad/s)

RC regulator, the extent of decreasing magnitude response becomes much smaller, which is 16dB when no bandwidth, 11dB when ω_c=2rad/s, 7dB when ω_c=5rad/s, 3dB when ω_c=10rad/s. Furthermore, the phase response at 300Hz also deviates from 0° when the grid frequency deviation happens. By comparing the four curves with different bandwidth, it can be found that when higher bandwidth is selected, the much smaller changing phase response can be observed, i.e., −55° to 55° when ω_c=10rad/s, −65° to 65° when ω_c=5rad/s, −75° to 75° when ω_c=2rad/s, −80° to 80° when ω_c=0rad/s. As a result, the closed-loop control performance of stator current harmonic suppression can deteriorate comparatively less when the higher bandwidth parameter is employed. Thus, it can be validated that the introduction of bandwidth in the proposed RBC regulator can be helpful to improve its robustness against grid frequency deviation from both the perspective of magnitude response and phase response, and the proposed BRC regulator can be more beneficial than the conventional RC regulator in the practical grid situation when grid frequency deviation occurs.

Fig.14 shows the control block diagram of the proposed stator current harmonic suppression strategy.

1) The PI regulator is used to control the fundamental component of rotor current. Since the rotor current control is implemented in dq^+ synchronous rotating frame, the rotor current control error always contains a DC component and 6*n* order AC signal components. The DC component can be restrained to zero by the PI regulator, while the 6*n* order AC error signals are automatically neglected due to the limited ac signal tracking capability of the PI regulator.

2) The BRC regulator is used to directly suppress the harmonic components of the stator current. The reference of BRC regulator is set as zero (meaning no harmonic components of stator current are expected to exist), and the stator current feedback I^+_{sdq} includes both DC and *6n* components of stator current. Since the DC component in the error signal unfortunately affects the harmonic control capability of the RC regulator[18], an additional high pass filter is used to remove the DC component in the stator current feedback.

The same experimental setup as described in Section 4 is used to validate the effectiveness of the proposed BRC regulator, and therefore a detailed description of the setup is not repeated. Fig.15 shows the experimental results of DFIG under high order harmonically distorted grid voltage condition with frequency of 50Hz when BRC control of stator current is disabled and the PI control of rotor current is enabled. The grid voltage distortion with abundant high order harmonic sequences results in the severely distorted DFIG stator current, i.e., harmonic components of 5.63% 5th, 4.14% 7th, 2.57% 11th, 1.99% 13th, 1.97% 17th, 1.86% 19th sequence, as listed in Table 4. Thus, it can be seen that DFIG operational performance can be significantly jeopardized if the harmonic suppression strategy is not implemented.

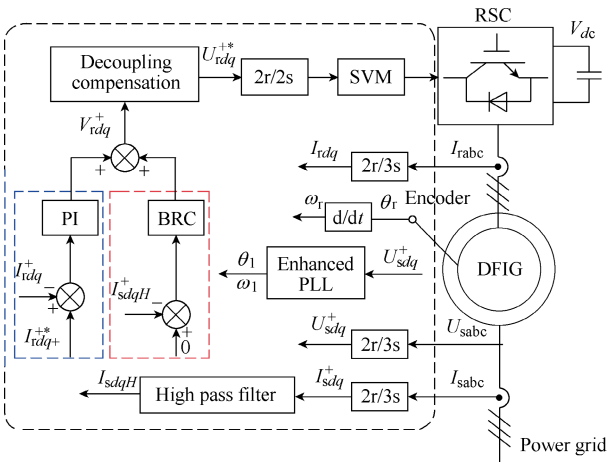

Fig.14 Block diagram of the proposed stator current harmonic suppression strategy

Table 4 Experiment result analysis data (%)

Frequency/ Hz	Grid voltage	BRC is disabled	50Hz, BRC ω_c=10rad/s	49.8Hz, Conventional RC	49.8Hz, BRC ω_c= 10rad/s
250	2.98	5.63	0.81	1.29	0.82
350	2.91	4.14	0.72	0.96	0.70
550	2.68	2.57	0.91	1.40	1.15
650	2.57	1.99	0.82	1.22	0.91
850	2.37	1.97	0.93	1.15	1.01
950	2.18	1.86	0.77	1.00	0.88

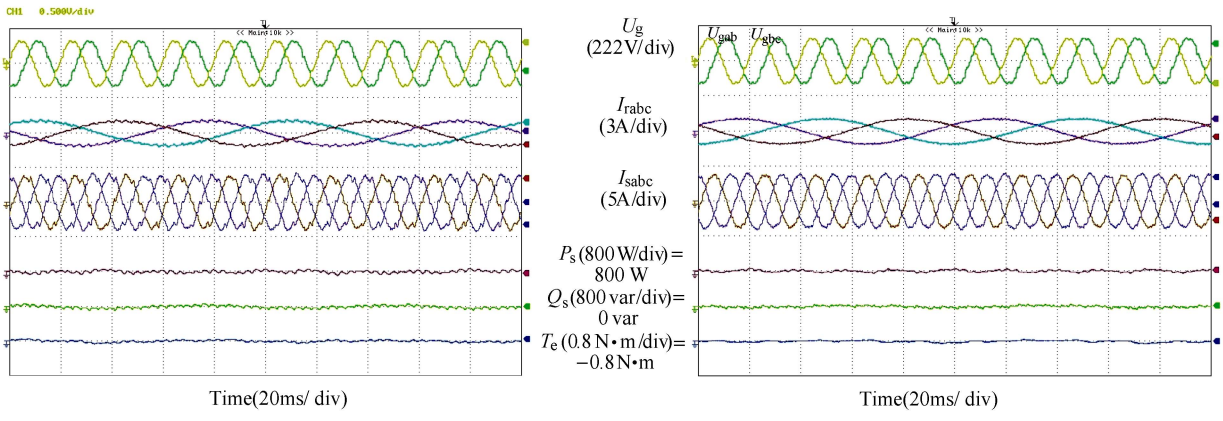

(a) Disabled (b) Enabled

Fig.15 Experimental result of DFIG under harmonically distorted grid voltage condition with frequency of 50Hz when BRC control of stator current is disabled and enabled

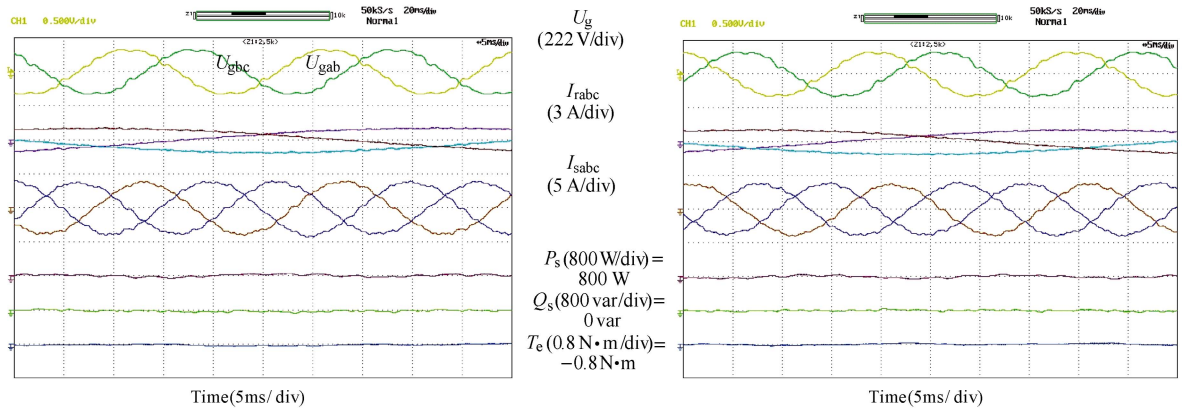

(a) Conventional RC regulator (b) BRC regulator with bandwidth ω_c=10 rad/s

Fig.16 Experimental result of DFIG under harmonically distorted grid voltage condition with frequency of 49.8Hz when conventional RC regulator or BRC regulator with bandwidth ω_c=10rad/s is proposed

Fig.16 shows the experimental result of DFIG under harmonically distorted grid voltage condition with frequency of 49.8Hz when Fig.16(a) conventional RC regulator or Fig.16(b) BRC regulator with bandwidth ω_c=10rad/s is proposed. As seen from Table 4, when conventional RC regulator is adopted in Fig.16(a), the stator current harmonic distortion includes 1.29% 5th, 0.96% 7th, 1.40% 11th, 1.22% 13th, 1.15% 17th, and 1.00% 19th sequence; while the BRC regulator with ω_c=10rad/s is adopted in Fig.16(b), the stator current harmonic distortion would include 0.82% 5th, 0.70% 7th, 1.15% 11th, 0.91% 13th, 1.01% 17th, and 0.88% 19th sequence. Thus, it can be seen from Table 4 that compared with the steady-state performance under normal frequency 50Hz, the steady-state performance with the conventional RC regulator and the BRC regulator under grid frequency deviation of 49.8Hz becomes worse. Moreover, it can also be validated that due to the introduction of bandwidth in the BRC regulator, the BRC regulator has higher magnitude response at the deviated control frequency, thus the better control capability of BRC regulator over conventional RC regulator can be guaranteed.

Above all, based on theoretical analysis and experimental results, it can be concluded that, compared with conventional RC regulator, the proposed BRC regulator can widen the effective control frequency spectrum by enlarging the magnitude response near the controlled frequency with the introduction of the bandwidth parameter, thus the BRC regulator is able to have superior robustness against the grid frequency deviation, and ensure the lower stator current harmonic components.

6 Conclusions

This paper starts with a combined compensation of the reactive power from back-to-back power converters in order to balance the lifetime distribution in the case of the normal grid condition. In the case of short-term grid fault, the challenges for DFIG to ride through the fault period is addressed, and an optimized demagnetizing current control is proposed to keep the minimum thermal stress of the power converter during the fault period. An improved control strategy of the DFIG system under unbalanced and distorted grid voltage is presented, with the control targets of the smooth active and reactive power or the balanced and sinusoidal current of the rotor-side converter and the grid-side converter. Finally, the control strategy of stator current harmonic distortion suppression by using the bandwidth based repetitive controller is discussed under generalized harmonic grid voltage, and it is proven that the proposed regulator has superior performance over the conventional repetitive controller, especially in the case of grid frequency deviation.

References

[1] Danish Energy Agency (website: http://www.ens.dk/en).

[2] H. Wang, M. Liserre, F. Blaabjerg, P. Rimmen, J. Jacobsen, T. Kvisgaard, and J. Landkildehus, “Transitioning to physics-of-failure as a reliability driver in power electronics,” *IEEE Journal of Emerging and Selected Topics in Power Electronics*, vol. 2, no.1, pp. 97-114, Mar. 2014.

[3] S. Yang, A. Bryant, P. Mawby, D. Xiang, L. Ran, and P. Tavner, “An industrial-based survey of reliability in power electronic converters,” *IEEE Trans. on Industrial Applications*, vol. 47, no. 3, pp. 1441-1451, May 2011.

[4] A. Wintrich, U. Nicolai, W. Tursky, and T. Reimann, “Application manual power semiconductors,” Semikron international GmbH, Nuremburg, 2011.

[5] F. Blaabjerg, and K. Ma, “Future on power electronics for wind turbine systems,” *IEEE Journal of in Emerging and Selected Topics in Power Electronics*, vol. 1, no. 3, pp. 139-152, Sep. 2013.

[6] H. Polinder, J. A. Ferreira, B. B. Jensen, A. B. Abrahamsen, K. Atallah, and R. A. McMahon, “Trends in wind turbine generator systems,” *IEEE Journal of Emerging and Selected Topics in Power Electronics*, vol.1, no.3, pp.174-185, Sep. 2013.

[7] North American wind power. Top 15 Wind turbine suppliers of 2013 revealed. (http://www.nawindpower.com)

[8] D. Zhou, F. Blaabjerg, T. Franke, M. Tonnes, and M. Lau, “Reduced cost of reactive power in doubly fed induction generator wind turbine system with optimized grid filter,” *IEEE Trans. on Power Electronics*, vol.30, no.10, pp. 5581-5590, Oct. 2015.

[9] J. Hu, Y. He, L. Xu, and B.W. Williams, “Improved control of DFIG systems during network unbalance using PI–R Current regulators,” *IEEE Trans. on Industrial Electronics*, vol. 56, no. 2, pp. 439-451, Feb. 2009.

[10] M. Tsili, and S. Papathanassiou, “A review of grid code technical requirements for wind farms,” *IET Renewable Power Generation*, vol. 3, no. 3, pp. 308-332, Sep. 2009.

[11] E.ON-Netz. Requirements for offshore grid connections, Apr. 2008.

[12] D. Zhou, F. Blaabjerg, M. Lau, and M. Tonnes, "Optimized reactive power flow of DFIG power converters for better reliability performance considering grid codes," *IEEE Trans. on Industrial Electronics*, vol. 62, no. 3, pp. 1552-1562, Mar. 2015.
[13] "Wind turbines– part I: design requirements", IEC 61400-1, 3rd edition.
[14] D. Xiang, L. Ran, P. J. Tavner, and S. Yang, "Control of a doubly fed induction generator in a wind turbine during grid fault ride-through," *IEEE Trans. on Energy Conversion*, vol. 21, no. 3, pp. 652-662, Sep. 2006.
[15] J. Lopez, E. Gubia, E. Olea, J. Ruiz, and L. Marroyo, "Ride through of wind turbines with doubly fed induction generator under symmetrical voltage dips," *IEEE Trans. on Industrial Electronics*, vol. 56, no. 10, pp. 4246-4254, Oct. 2009.
[16] D. Zhou, and F. Blaabjerg, "Minimum junction temperature swing for DFIG to ride through symmetrical voltage dips," in *Proc. of ECCE 2015*, pp. 493-499, 2015.
[17] D. Chen, J. Zhang, and Z. Qian, "Research on fast transient and 6*n*±1 harmonics suppressing repetitive control scheme for three-phase grid-connected inverters," *IET Power Electron.*, vol. 6, no. 3, pp. 601–610, 2013.
[18] Y. Song, and H. Nian, "Sinusoidal output current implementation of DFIG using repetitive control under a generalized harmonic power grid with frequency deviation," *IEEE Trans. on Power Electronics*, vol. 30, no. 12, pp. 6751-6762, Dec. 2015.
[19] J. Hu, H. Nian, H. Xu, and Y. He, "Dynamic modeling and improved control of DFIG under distorted grid voltage conditions," *IEEE Trans. on Energy Conversion*, vol. 26, no. 1, pp. 163-175, Mar. 2011.
[20] J. Hu, H. Xu, and Y. He, "Coordinated control of DFIG's RSC and GSC under generalized unbalanced and distorted grid voltage conditions," *IEEE Trans. on Industrial Electronics*, vol. 60, no. 7, pp. 2808-2819, Jul. 2013.
[21] H. Xu, J. Hu, and Y. He, "Integrated modeling and enhanced control of DFIG under unbalanced and distorted grid voltage conditions," *IEEE Trans. on Energy Conversion*, vol. 27, no. 3, pp. 725-736, Jul. 2012.
[22] Van-Tung Phan, and Hong-Hee Lee, "Control strategy for harmonic elimination in stand-alone DFIG applications with nonlinear loads," *IEEE Trans. on Power Electronics*, vol. 26, no. 9, pp. 2662-2675, Sep. 2011.
[23] H. Xu, J. Hu, and Y. He, "Operation of wind-turbine-driven DFIG systems under distorted grid voltage conditions: analysis and experimental validations," *IEEE Trans. on Power Electronics*, vol.27, no.5, pp. 2354-2366, May 2012.
[24] H. Nian, and Y. Song, "Direct power control of doubly fed induction generator under distorted grid voltage," *IEEE Trans. on Power Electronics*, vol. 29, no. 2, pp. 894-905, Feb. 2014.
[25] C. Liu, F. Blaabjerg, W. Chen, and D. Xu, "Stator current harmonic control with resonant controller for doubly fed induction generator," *IEEE Trans. on Power Electronics*, vol. 27, no. 7, pp. 3207-3220, Jul. 2012.

Dao Zhou (S'12, M'15) received the B.S. in electrical engineering from Beijing Jiaotong University, Beijing, China, in 2007, the M. S. in power electronics from Zhejiang University, Hangzhou, China, in 2010, and the Ph.D. from Aalborg University, Aalborg, Denmark, in 2014.

He is currently a Postdoctoral Researcher in Aalborg University. His research interests include power electronics and reliability in renewable energy application.

Dr. Zhou received the Renewable and Sustainable Energy Conversion Systems of the IEEE Industry Applications Society First Prize Paper Award in 2015, and Best Session Paper at Annual Conference of the IEEE Industrial Electronics Society (IECON) in Austria in 2013. He serves as a Session Chair for various technical conferences.

Yipeng Song was born in Hangzhou, China. He received the B.S. degree and Ph.D. degree both from the College of Electrical Engineering, Zhejiang University, Hangzhou, China, in 2010 and 2015. He is currently working as a Postdoc at the Department of Energy Technology in Aalborg University, Denmark. His current research interests are motor control with power electronics devices in renewable-energy conversion, particularly the control and operation of doubly fed induction generators for wind power generation.

Frede Blaabjerg (M'88–SM'97–F'03) was with ABB-Scandia, Randers, Denmark, from 1987 to 1988. From 1988 to 1992, he was a Ph.D. student with Aalborg University, Aalborg, Denmark. He became an Assistant Professor in 1992, Associate Professor in 1996, and Full Professor of power electronics and drives in 1998. His current research interests include power electronics and its applications such as in wind turbines, PV systems, reliability, harmonics and adjustable speed drives.

He has received 17 IEEE Prize Paper Awards, the IEEE PELS Distinguished Service Award in 2009, the EPE-PEMC Council Award in 2010, the IEEE William E. Newell Power Electronics Award 2014 and the Villum Kann Rasmussen Research Award 2014. He was an Editor-in-Chief of the IEEE TRANSACTIONS ON POWER ELECTRONICS from 2006 to 2012. He is nominated in 2014 and 2015 by Thomson Reuters to be between the most 250 cited researchers in Engineering in the world.